https://doi.org/10.5194/nhess-2021-111
Preprint. Discussion started: 28 April 2021

Natural Hazards and Earth System Sciences
Discussions

A data-driven evaluation of post-fire landslide susceptibility

Elsa S. Culler[1, 2], Ben Livneh[1, 2], Balaji Rajagopalan[1], and Kristy F. Tiampo[3, 2]

[1]University of Colorado Boulder Department of Civil, Architectural, and Environmental Engineering
[2]Cooperative Institute for Research in Environmental Sciences (CIRES), University of Colorado Boulder
[3]University of Colorado Boulder Department of Geologic Sciences

Correspondence: Elsa Culler (elsa.culler@colorado.edu)

Abstract. Wildfires change the hydrologic and geomorphic response of watersheds, which has been associated with cascading hazards that include shallow landslides and debris flows. This study evaluates post-wildfire landslide trigger characteristics by comparing precipitation preceding landslides at both burned and unburned locations. Landslide events are selected from the NASA Global Landslide Catalog (GLC) to facilitate regional inter-comparison. Fire and precipitation histories for each site are established using MODIS global burned area and CHIRPS precipitation data, respectively. Analysis of normalized seven-day accumulated precipitation for sites across all regions shows that, globally, landslides at burned sites are preceded by less precipitation than landslides without antecedent burn events. This supports the hypothesis that fire increases rainfall-driven landslide hazards. An analysis of the seasonality of landslides at burned and unburned locations shows that landslide-triggering storms in burned locations tend to exhibit different seasonality from other rainfall-triggered landslides, with a variety of seasonal shifts ranging from approximately six months in the Pacific Northwest of North America to one week in the Himalaya region. Overall, this manuscript offers an exploration of regional differences in the characteristics of rainfall-triggered landslides over a broad spatial scale and encompassing a variety of climates, geographies, and burn conditions.

1 Introduction

Landslides can be destructive to people, property and infrastructure in their paths. Worldwide, these natural disasters cause tens of thousands of deaths each year (Froude and Petley, 2018). Landslide mitigation costs in the United States (US) are approximately 2 billion USD annually, with worldwide costs much higher (Schuster and Highland, 2001). Though an accurate assessment of landslide hazards would aid mitigation efforts (Spiker and Gori, 2002), such an evaluation presents a challenge in part because landslides are often triggered by a sequence of cascading natural hazards (Klose, 2015a). For example, landslides may interact with other complex phenomena such as heavy rain, wildfires, floods, earthquakes, melting permafrost and glacial outbursts (Budimir et al., 2015; Harp et al., 2011; Kirschbaum et al., 2020, 2012; Rupert et al., 2003).

Here, we focus on a particular sequence of cascading natural hazards: the post-wildfire landslide. In these events, wildfires are followed by intense precipitation leading to mass movements such as a sediment-laden floods, shallow landslides, or debris flows. The impact of wildfire on landslide hazards can vary on the basis of static factors such as burn severity, vegetation, and soil types (Shakesby et al., 1993; Moody et al., 2018). Post-wildfire landslide hazards may also depend on dynamic factors such as soil moisture, meteorology and the length of time since the most recent fire (Kirschbaum and Stanley, 2018). There

https://doi.org/10.5194/nhess-2021-111
Preprint. Discussion started: 28 April 2021


Natural Hazards and Earth System Sciences Discussions

are numerous local studies demonstrating a relationship between wildfire and the amount of precipitation that triggers a mass movement (Cannon et al., 2008; Gartner, 2005; Reneau et al., 2007). However, the lack of complete landslide inventories including a wide variety of climates and ecoregions presents an obstacle to a general evaluation of the role of fire in rainfall-triggered landslides (Klose, 2015b).

This study seeks to test the hypothesis that wildfire increases landslide susceptibility at the regional scale by detecting and characterizing differences in landslide-triggering precipitation at both burned and unburned sites. The relative magnitude of triggering precipitation is used here as a proxy for landslide susceptibility using a large sample of landslides ($n = 5313$) across six global regions.

1.1 Mechanisms by which fire increases landslide hazards

While many factors contribute to landslide hazards, only a subset are altered by fire exposure (Highland and Bobrowsky, 2008), which are of interest to this analysis. Fire changes the hydrologic and geomorphic response through several distinct physical mechanisms. First, the destruction of vegetation contributes to the development of debris flows and other mass movements in three ways:

- Sediment gathered behind vegetation trunks and stems can, after a fire, be mobilized either by a rain storm or as dry ravel, i.e. sediment that rolls down the slope without precipitation (Cannon and Gartner, 2005).
- Vegetation destruction clears pathways for water and sediment to flow downhill more quickly (Shakesby and Doerr, 2006).
- Following a fire, canopy and litter storage - water that gets trapped in leaves and other detritus on the ground - is greatly reduced, resulting in increased runoff and sediment transport (Cannon and Gartner, 2005; Shakesby and Doerr, 2006).

Additionally, soil properties can be dramatically altered post-fire, resulting in the following three effects which also contribute to the formation of mass movements such as debris flows:

- Burned soils can have reduced organic content as a result of the combustion process, which causes them to have reduced water-holding capacity (Neary et al., 2005).
- Combustion of organic content also typically reduces soil aggregate stability, promoting erosion (Shakesby and Doerr, 2006).
- Some combinations of soil, vegetation type, and temperature can decrease wettability or produce a hydrophobic layer 1-5 cm beneath the soil, thereby dramatically increasing runoff (Spittler, 1995). The implications of this effect vary dramatically from place to place, since fire can also destroy hydrophobic layers in the right conditions (Shakesby and Doerr, 2006). In addition, these effects are not always uniform across the burned area, and the effects of changed wettability can last from days to years depending on the local conditions (Shakesby and Doerr, 2006).

https://doi.org/10.5194/nhess-2021-111
Preprint. Discussion started: 28 April 2021


Natural Hazards and Earth System Sciences Discussions

- A layer of post-fire ash caused by fire can also result in a large reduction in infiltration, although it can also increase soil storage potential depending upon the thickness and hydraulic conductivity of the layer (Ebel et al., 2012).

- One consequence of wildfire-driven changes to soil and vegetation on rainfall-triggered landslides is that the predominant mechanism shifts from infiltration-driven to runoff-driven (Cannon and Gartner, 2005). Infiltration-driven landslides are typically shallow slope failures initiated by longer storms that saturate the shallow subsurface. By contrast, runoff-driven landslides are often debris flows caused by high-volume storms that mobilize sediment on the surface without the need for much infiltration. Landslides can often be identified as one type or another primarily by observing whether the landslide had a point origin, as with infiltration-driven landslides, or a distributed origin like runoff-driven landslides. For infiltration-driven landslides, the antecedent soil moisture conditions are more important for evaluating landslide hazards since soil saturation is fundamental to the mechanism of slope failure. However, post-wildfire landslides, tend to be less driven by infiltration since the hydrophobic and more erodible sediment layer creates an ideal condition for runoff-driven landslides. (Cannon and Gartner, 2005).

1.2 Evidence for increased landslide hazards with increased burn severity

Wildfire has been empirically linked to increased frequency and volume of debris flows in several regions of the Western US (Cannon and Gartner, 2005). A key piece of evidence for this connection comes from a series of studies based on repeated post-storm observations of burned watersheds in Southern California and the Intermountain West regions of the US as part of the development of the US Geological Survey's (USGS) operational post-wildfire landslide hazard predictions (Cannon et al., 2010; Gartner et al., 2009, 2014; Rupert et al., 2003; Staley et al., 2016). These five studies model the probability of landslides following fire using logistic regressions to demonstrate that both burn severity (Staley et al., 2016) and burn extent within a watershed (Cannon et al., 2010) are associated with increased debris flow likelihood. Gartner et al. (2014) found that the increase in landslide probability in a watershed due to wildfire is greatest immediately after wildfire, but can last a total of 2-5 years. Increased likelihood of post-wildfire debris flows has also been associated with the erodibility of fine sediment in the soil, soil organic matter percentage, soil clay percentage, underlying lithology (e.g. sedimentary or granitic rock), watershed area, and watershed relief ratio (Gartner et al., 2009; Rupert et al., 2003).

The statistically significant positive relationship between landslides and burn severity strongly suggests that landslide susceptibility increases after wildfires in the Western US, although none of the above studies include observations of unburned sites as a control. Instead, the databases used in Cannon et al. (2010); Gartner et al. (2009, 2014); Rupert et al. (2003); Staley et al. (2016) include multiple observations of the presence or absence of a debris flow at each site, making them suitable for a regression analysis based on burn severity, but not for comparing burned and unburned locations. In addition, while these post-wildfire landslide observations contain precise dates and locations, and extend across a remarkable spatial range when compared to most other landslide hazard models, they still are limited to 119 sites or fewer (Gartner et al., 2014). This limited spatial extent leaves open the question of whether the fire-flood patterns of the Western US are unique, or if similar hazards are just as ubiquitous but under-reported in other regions.

https://doi.org/10.5194/nhess-2021-111
Preprint. Discussion started: 28 April 2021


Natural Hazards and Earth System Sciences
Discussions

1.3 Sources and methods for landslide data collection

It is resource-prohibitive to conduct a continuous systematic search for mass movements either in the field or with satellite observations. As a result, many of the most accurate and complete methods for systematically identifying landslides can presently only be used over limited spatial and temporal domains. For example, Lee and Pradhan (2007) identified landslides from aerial photograph interpretation and a field survey over the ~ 800 km^2 Selangor area in Malaysia, and Nefeslioglu et al. (2010), used an inventory based on aerial photographs taken in 1955-1956 to analyze landslide susceptibility over a ~ 175 km^2 area near Istanbul, Turkey. An alternative to manual identification either in the field or using photographs is automatic or semi-automatic landslide detection using image processing on aerial imagery, LiDAR surveys, or Synthetic Aperture Radar (SAR). These automated methods are typically applied over similarly small domains due to challenges with obtaining imagery and compiling training datasets. For example, Martha et al. (2013) used aerial imagery over ~ 120 km^2 in the Himalayas, while Mezaal et al. (2017) used LiDAR over the 26.7 km^2 Cameron Highlands of Malaysia. SAR interferometry can be used for identification of pre-landslide motion, as was done by Lu et al. (2012) over the ~ 1500 km^2 Arno basin in Italy. In addition, several SAR techniques have been employed to identify post-landslide scars, including SAR amplitude mapping of landslides triggered by the Gorkha, Nepal earthquake in 2015 over a $14,500$ km^2 area (Meena and Tavakkoli Piralilou, 2019), coherence mapping of interferometric SAR the same earthquake-triggered landslides (Burrows et al., 2019), and the wildfire-triggered landslides over ~ 60 km^2 of the area burned by the 2017 Thomas Fire in California (Donnellan et al., 2018). While automated landslide detection as deployed in the above studies is continually undergoing promising advances, at the time of this analysis it has not yet been used to compile an inventory over a broad enough spatial domain to facilitate inter-regional comparisons. Such records collected in an uncoordinated effort over small domains are unsuitable for regional inter-comparisons such as we have undertaken here because these records do not contain standardized information for every region, are often unpublished (van Westen et al., 2006), and are unlikely to have daily temporal resolution that would allow comparison with the precipitation record (Kirschbaum et al., 2010).

For this study, we chose to use the NASA Global Landslide Catelog (GLC, Kirschbaum et al., 2010). As with the few other regional and global databases available, the broad domain of the GLC comes coupled with issues of precision and completeness. The sources of GLC data are second-hand observations made by the news media, governmental organizations such as departments of transportation, and some available scientific reports (Kirschbaum et al., 2010). The absence of a systematic search for landslides across the entire database domain results in a substantial spatial bias towards populated areas where landslides happen to be noticeable. News reports also suffer relatively high location uncertainty (as much as 50 km) depending on how specific the source article is about the location (Kirschbaum et al., 2010). Finally, though the GLC does contain some information about the landslide mechanisms that would allow landslides to be classified, for example, as debris flows or shallow landslides, these data may not be reliable since they are not based on direct observations. Despite limitations in accuracy and completeness, the GLC was chosen for this study primarily because as of this writing it offers the largest spatial and temporal range of any catalog. The GLC contains a large sample of landslides at unburned control basins from across the

https://doi.org/10.5194/nhess-2021-111
Preprint. Discussion started: 28 April 2021


Natural Hazards and Earth System Sciences Discussions

globe ($n = 5313$) as well as a substantial proportion of landslides identified in this study as having occurred in recently burned areas ($n = 489$; $9.2\,\%$).

1.4 Towards a global picture of global landslides susceptibility

This study seeks to test the hypothesis that wildfires increase landslide susceptibility by evaluating antecedent precipitation at both burned and unburned landslides locations. Some existing local and regional studies (Cannon et al., 2010; Rupert et al., 2003) have assessed the impact of wildfire on landslide susceptibility, but have not included unburned locations in their analyses. Other studies have also featured the GLC data and a global spatial extent, with a focus on validating large-scale landslide hazard models (Kirschbaum and Stanley, 2018). This analysis is unique from other regional and global studies in that it combines the broad scope of the GLC data with an exploration of the role of wildfire in landslide susceptibility. This study is also distinct from others that focus on the role of wildfire on landslide sites (Gartner et al., 2009) in that here burned sites are contrasted with unburned sites instead of previous observations of the same location. Finally, in contrast to post-wildfire landslide studies focused on a specific regions like the western US (Cannon and DeGraff, 2009), southern California (Gartner et al., 2014), or southeast Australia (Nyman et al., 2011), this study combines the GLC with globally-observed fire and precipitation data to offer unique insights into the role of fire on landslide susceptibility in diverse regions across the globe.

2 Methods

We first describe the landslide data (Sect. 2.1), the study regions (Sect. 2.2) and fire data (Sect. 2.3). The precipitation data (Sect. 2.4) leading up to the date of each landslide were compared using three approaches. First, the seven-day running total precipitation depth percentile (see Sect. 2.4) in the weeks preceding each landslide was used as a proxy for landslide susceptibility. This percentile value was compared between burned and unburned sites within each region and for all included landslides (see Sect. 2.5). Next, seven-day precipitation percentiles were compared with bootstrapped samples from burned and unburned sites separately (see Sect. 2.6) to confirm the findings from the depth percentile analysis and also to draw out differences in storm timing between burned and unburned groups. Finally, the precipitation frequency in the burned and unburned groups in the months and years surrounding each landslide (see Sect. 2.7) was examined to identify shifts in the seasonality of landslides at burned sites relative to the unburned group. These seasonality results were augmented with kernel density estimates of landslide occurrence by day-of-year at burned and unburned sites for each region.

2.1 Landslide data

A large sample ($n = 5313$) of rainfall-triggered landslides was obtained from the GLC. Landslide locations are shown in Fig. 1, along with a summary of fire and precipitation information obtained for those locations from the sources listed in Table 1 (see Sects. 2.3 and 2.4). The GLC provides a large collection of events taking place in a variety of climates such that, in combination with spatially continuous observations of fire (500m Moderate Resolution Imaging Spectroradiometer [MODIS] Burned Area by Giglio et al., 2018) and precipitation (5.5km Climate Hazards group InfraRed Precipitation with Station data

https://doi.org/10.5194/nhess-2021-111
Preprint. Discussion started: 28 April 2021

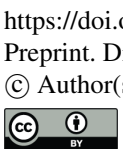

Natural Hazards and Earth System Sciences
Discussions
Open Access
EGU

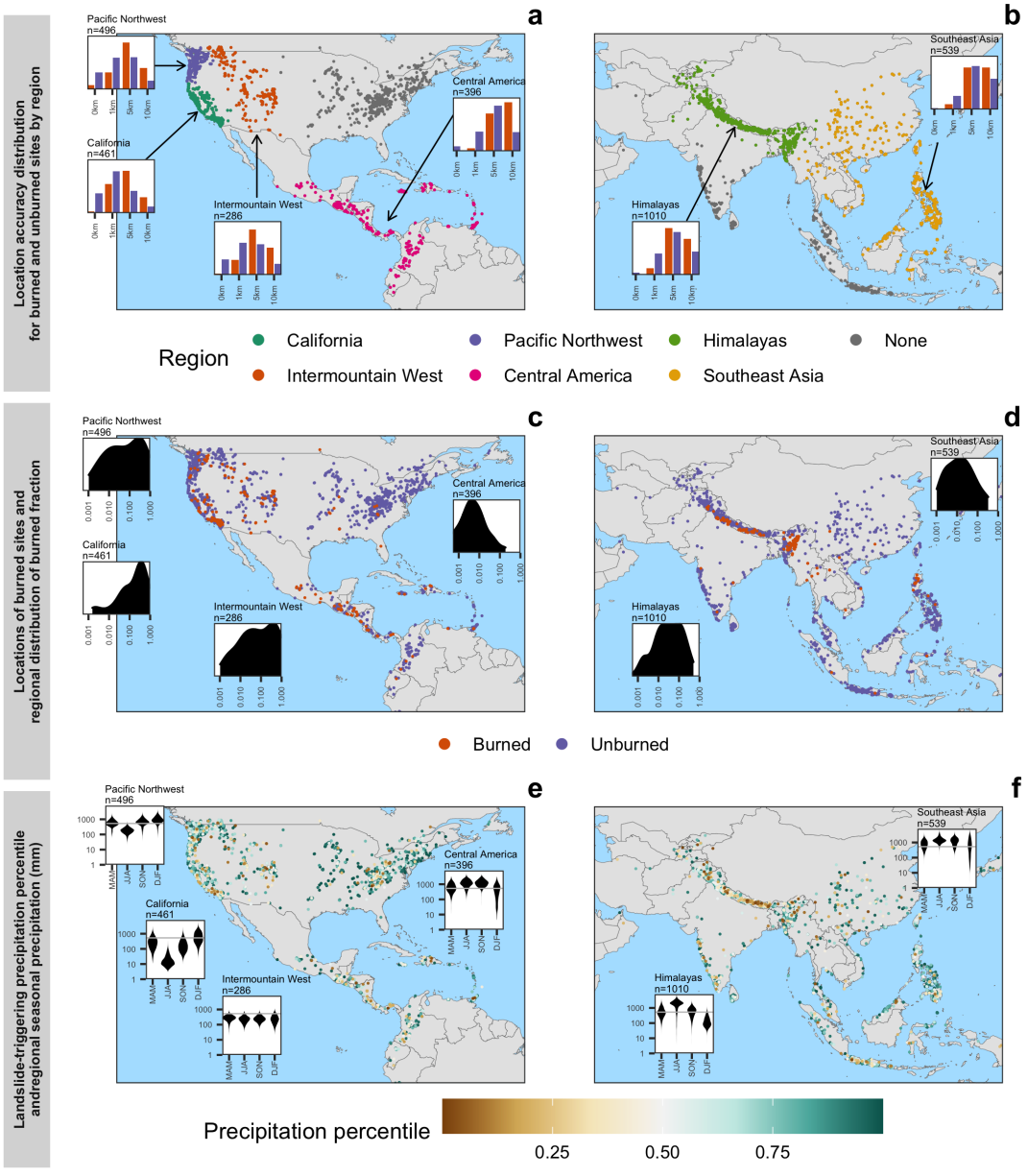

Figure 1. Landslide locations ($n = 5313$, $2006 - 2017$), showing region coding (see Sect. 2.2) in (a) and (b), with location accuracy for burned and unburned groups in the regional insets; burned/unburned classification at the time of the landslide in (c) and (d), with regional insets showing kernel density portrayal of the fraction of burned area for the landslide locations from the three years preceding the landslide; and the precipitation percentile on the day of the landslide in (e) and (f), with regional insets of kernel density estimates (violin plots) of the climatological ($1981 - 2020$) seasonal precipitation magnitude (mm) including a reference line indicating the median seasonal average across all sites globally. Country boundaries were obtained from the maps R package (Deckmyn et al., 2018)

https://doi.org/10.5194/nhess-2021-111
Preprint. Discussion started: 28 April 2021


Natural Hazards and Earth System Sciences
Discussions

[CHIRPS] by Funk et al., 2015) data, it is well suited for comparing the diverse precursors under which post-wildfire landslides occur.

In order to reduce errors resulting from including a variety of types of rainfall-triggered landslides within the same dataset, the selected landslides were limited to those categorized by a 'landslide trigger' value of 'rain,' 'downpour,' 'flooding,' or 'continuous rain.' Landslides with a second trigger such as an earthquake were eliminated. Snowmelt-driven landslides were also not included because the impact of precipitation is delayed in those cases – an analysis of the snow record in California/Nevada revealed only a single event with enough antecedent snow to suggest it could have been mislabeled. Only records that were indicated to have occurred within a radius of 10 km or less of the recorded location were included, since the landslides with lower location accuracy presented problems for wildfire classification. In addition, only landslides between $50°$S and $50°$N latitude were included, and the events occurring before the year 2000 were omitted, so as to ensure coverage by both fire and precipitation datasets (see Table 1).

2.2 Study regions

To compare the differences in landslide triggers in different climates, we divided the landslides into regions (see Fig. 1 panels (a)and (b)). Regions were determined using the AGglomerative NESting (AGNES) hierarchical clustering algorithm (Kaufman and Rousseeuw, 2009) considering the latitude and longitude of the landslides, and clusters were subsequently combined, split, or eliminated on the basis of sample sizes as described below. First, the cluster tree was truncated at 30 clusters, after which all the clusters with fewer than 100 data points or less than $5\,\%$ burned sites were eliminated. Cases where two nearby regions with lower numbers of landslides, for example, Central America and Caribbean/Venezuela, were joined manually. Finally, the largest region, encompassing Western US and Canada, was split into three sub-regions based on an additional identical clustering process over this sub-domain. The final regions are shown in Fig. 1 panel (a). The Pacific Northwest of North America was included even though the percentage of burned sites is lower than threshold, but at $4.4\,\%$ it was nearly double the highest percentage among the eliminated regions ($2.25\,\%$ in the Eastern US). Some landslides were not included in any of the final regions. These events were not, however, eliminated from any analysis of all landslides.

2.3 Fire data

For each landslide, a circle centered at the landslide location and with a radius of the location accuracy was computed and each $500\,$m pixel within the circle was extracted from the MODIS Burned Area dataset (Giglio et al., 2018). Fire affects the landscape over a large range of temporal scales in different settings. Previous studies suggest that the post-wildfire increase in landslide susceptibility peaks within the first six months, but that a second time period of increased susceptibility can appear at 3 years or even longer (DeGraff et al., 2015; Gartner et al., 2014). Landslides were classified as burned if any part of the area where the landslide occurred was burned at some point within the three years prior to the event to capture both waves of increased susceptibility without over-identifying landslides areas where fires occur every few years. The fraction of pixels that were burned over the 3-year antecedent period was then computed, and landslides classified as burned if there was any overlap

https://doi.org/10.5194/nhess-2021-111
Preprint. Discussion started: 28 April 2021

Natural Hazards and Earth System Sciences
Discussions
Open Access
EGU

Table 1. Description of datasets used in the analysis

Data source	Description	Spatial extent	Spatial Resolution	Temporal Range	Temporal Resolution
NASA Global Landslide Catalog (GLC; Kirschbaum et al., 2010)	Compilation of landslides drawn from news articles and scientific reports	Global, with variable coverage in different countries	Landslide location accuracy varies from exact to 50 km range. The coarsest location accuracy used was 10 km.	1988–2015, most data 2007–2015	Daily for most data points
Climate Hazards Infrared Precipitation with Stations (CHIRPS) (Funk et al., 2015)	Station-corrected gridded precipitation data derived from cloud temperature observed using infrared satellite observations	$50°$S to $50°$N	$0.05°$ (~ 5.5 km)	1981–2020	Daily
MODIS Burned Area (Giglio et al., 2018)	Dates on which a pixel was burned, derived from NASA's MODIS Terra and Aqua satellites. The product uses a reprocessing algorithm that combines changes in burn-sensitive vegetation index and active fire locations.	global	500 m	2000–2020	Daily
Daymet Precipitation and Snow Water Equivalent (Thornton et al., 2014)	An alternative precipitation dataset based on station data and topographic information	North America	1 km	1980–2020	Daily

https://doi.org/10.5194/nhess-2021-111
Preprint. Discussion started: 28 April 2021


Natural Hazards and Earth System Sciences Discussions

between burned areas and the landslide circle. As a result of this analysis, 489 landslides (9.2 %) were categorized as potential post-wildfire events.

While this method of identifying post-wildfire landslides ensured that all post-wildfire landslides were classified as burned, the low spatial accuracy of many of the landslide locations leaves open the possibility that some landslides occurred near a recent fire but not within the fire perimeter. For this reason we refer to landslides as 'burned' instead of post-wildfire in this analysis. This type of error is a function of both the burned fraction and the conditional probability of landslide occurrence given that a fire has occurred. False positives are therefore less likely for landslides with better location accuracy, which made up a larger proportion of landslides in the regions within the US and Canada than other regions. Fig. 1 shows the distributions of burned fractions for each region. Note that in Central America and Southeast Asia, very few sites have above 10 % burned fraction (see Fig. 1 panels (c) and (d) inset plots). This could be due to those regions having lower landslide location accuracy, resulting in a higher likelihood of false positive post-wildfire landslides.

2.4 Precipitation data

Time series of precipitation at the landslide sites were obtained from the CHIRPS precipitation dataset (Funk et al., 2015). Precipitation was averaged for each landslide location within the radius of the provided location accuracy. Additional pre-processing steps described below were performed to distinguish anomalously high precipitation events from potential seasonal shifts and climatic differences across sites.

A 7-day running average of antecedent precipitation was computed to enable direct comparison of landslides triggered by storms of different lengths and intensities. While including an estimate of the soil moisture was outside the scope of this study, 7-day antecedent rainfall indices have been used by other modelling studies as a surrogate for soil moisture in a combined indicator of landslide susceptibility (James and Roulet, 2009; Kirschbaum and Stanley, 2018). In addition to allowing a more equal comparison of landslide triggers which fall within throughout this spectrum of storm intensity, the running average is less sensitive to small errors in precipitation and landslide date accuracy. Figure 1 panels (e) and (f) show these 7-day cumulative-precipitation percentiles, as well as the climatological seasonal average precipitation, revealing that the Western US is dominated by dry summers, while the lower-latitude regions exhibit wetter summers and in some cases monsoons.

We further screened landslide events with no recorded precipitation in advance of reportedly rainfall-triggered landslides. Figure 2 shows a quality control sub-analysis for the California/Nevada area to investigate the need for data screening on the basis of inconsistencies between the landslide and precipitation record. This region was chosen for the quality control analysis, because of its high density of precipitation data and variety of climate conditions, useful for identifying erroneous landslide precipitation. We found 14 % (73 of 533) of the landslides in this region had no triggering precipitation event recorded in the CHIRPS data. Since the GLC contains only rainfall-triggered landslides, the lack of precipitation in these cases was likely a result of errors in either the precipitation data or landslide data. A comparison with the Daymet precipitation dataset over the same domain revealed that the two precipitation datasets frequently did not agree on these zero-precipitation landslide events, suggesting that the problem largely originated from the precipitation data themselves. Furthermore, the concentration of data points on the x and y axes of Fig. 2 suggests that disagreements on precipitation occurrence are distinct from disagreements on

https://doi.org/10.5194/nhess-2021-111
Preprint. Discussion started: 28 April 2021

Natural Hazards and Earth System Sciences
Discussions

the non-zero amounts of precipitation and potentially a separate source of error. To limit the effect of these inconsistent data points on the results, all landslides worldwide with no measured precipitation in the six days before and one day after the event were removed from the global study (367 of 5680 or 6.5 % removed for a final $n = 5313$).

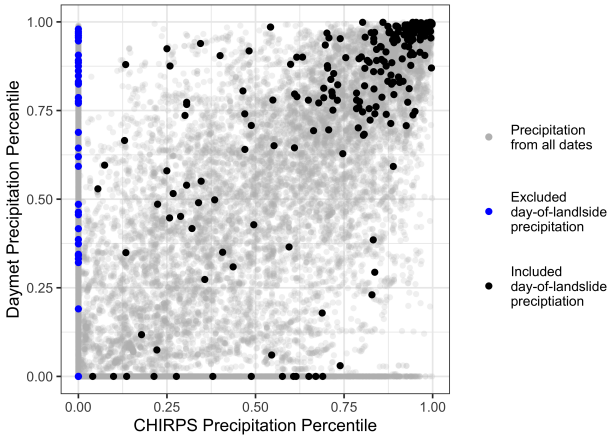

Figure 2. Seven-day precipitation percentiles for Daymet versus CHIRPS products computed for the six days before and one day following recorded California/Nevada landslides. Blue and black points show the screened and included landslides, respectively, whereas cumulative precipitation from the rest of the available record is shown in grey.

Precipitation data were further processed to facilitate the comparison of landslide-triggering events across a variety of seasons and climates. To facilitate inter-site precipitation comparison, the 7-day precipitation values were normalized for both location and time of year by computing a 30-day rolling percentile based on 38 years of historical precipitation climatology from 1981–2019 for each location. The percentile was computed from all the precipitation values from up to 15 days before or after the day of the year (DOY) on which the landslide occurred, and from all years in the record. This statistic controls for geographic and seasonal differences across landslide events by producing a normalized precipitation distribution that remains uniform for location and time of year. As a result, anomalous precipitation events are highlighted, facilitating the comparison of landslide triggers across locations and seasons.

2.5 Precipitation percentile experiment

This experiment compares the 7-day precipitation percentile in the burned and unburned groups in the time leading up to a landslide. The percentile indicates the degree to which landslide-triggering storms were exceptionally large and also serves as a proxy for relative landslide susceptibility. A one-sided Mann–Whitney hypothesis test was used to ascertain whether the precipitation percentiles of burned sites were less than the precipitation percentiles of unburned sites. Deviations between the burned and unburned groups defined by a p–value less than 0.05 on the Mann–Whitney test indicate statistically significant differences in the landslide susceptibility of the two groups. The null hypothesis of the Mann–Whitney test was that the median percentile of the burned sites is greater than or equal to the median percentile of the unburned sites. The precipitation per-

https://doi.org/10.5194/nhess-2021-111
Preprint. Discussion started: 28 April 2021


Natural Hazards and Earth System Sciences Discussions

centile distributions of all 7-day periods with non-zero precipitation are uniformly distributed as a result of the pre-processing described in Sect. 2.4, making the Mann–Whitney test the most appropriate hypothesis test. However, since zero-precipitation periods are excluded, this method cannot account for differences in the frequency of precipitation across different climates, but rather reflects differences in the magnitude of 7-day precipitation totals.

2.6 Bootstrapped samples experiment

In order to evaluate how anomalous the precipitation events preceding burned and unburned landslides were to "typical" local climate conditions at the landslide locations, we compared them to bootstrapped samples from other years to obtain a clearer signal. One hundred samples were taken from the 38-year precipitation records to match the locations and DOY of the observed landslides, but from randomly selected years ($n \approx 100$ for the individual samples, with the actual sample number adjusted by region so that all sites were selected evenly). Sampling was repeated for burned and unburned groups within each region as well as for all the landslides in the study. These samples are representative of precipitation for a particular lead time at the landslide locations and serve as a control dataset with which to compare the pre-landslide precipitation. Next, the observed landslide-year precipitation across all sites in the group was tested against each bootstrap sample using a Mann–Whitney test, with the null hypothesis that the sample median was less than or equal to the median of the precipitation percentiles from that day of the year in the entire record from 1981–2020. This produced a distribution of p–values that represent the likelihood that the precipitation leading up to the landslides varied from the control baseline.

This sampling method, though more complex, helps to reduce noise in the hypothesis test results due to different sample sizes in different regions. It also provides more information on general landslide susceptibility of each region rather than only the relative susceptibility of burned and unburned sites. Finally, it includes measurements of zero precipitation, which were eliminated from the direct comparison because of long-term climatic differences in precipitation frequency between burned and unburned sites in all regions.

2.7 Landslide seasonality experiment

To investigate the potential role of wildfires in affecting landslide seasonality, we estimated precipitation frequency at the landslide sites over time by computing the fraction of sites in the burned and unburned groups that had precipitation on any given day. As with the percentiles and the bootstrap p–values, frequency estimates were computed relative to the landslide event rather than by calendar date, resulting in time coordinates measured in 'years before the landslide'. Precipitation frequency was estimated for two years before and after the landslide in order to highlight changes in the magnitude and phase of the precipitation pattern. We found that in most regions there was a long-term difference in the mean annual frequency, likely because fires occur more often in areas with drier climates (Liu et al., 2014). These persistent differences between burned and unburned sites were removed by subtracting the mean precipitation frequency for both the burned and unburned groups. Finally, we took a 90-day running average to reduce noise in the data and thereby make it easier to visually identify any long-term shifts in landslide occurrence. These frequency estimates are not normalized by season, which means that unlike the previous two

https://doi.org/10.5194/nhess-2021-111
Preprint. Discussion started: 28 April 2021


Natural Hazards and Earth System Sciences Discussions

metrics they can be used to compare the degree of shift in the seasonality of landslides at burned versus unburned sites relative to annual precipitation cycles.

Additional seasonality analysis was performed to provide insight into the times of year that landslides occur at burned versus unburned sites. Kernel density estimates of landslide occurrence throughout the year were compared between the burned and unburned groups. This seasonality analysis would highlight a shift from Fall to Spring but, in contrast with the frequency analysis, it does not indicate the precipitation conditions under which landslides typically occur. Together, the frequency and seasonality analyses can show both the seasonal shift as well as any changes in landslide occurrence relative to annual precipitation patterns.

3 Results

3.1 Precipitation percentile experiment

The distributions of precipitation event percentiles for all the included landslides are shown in Fig. 3. The precipitation percentile increases for all groups as the date of the landslide approaches, confirming that these rainfall-triggered landslides are generally preceded by an increase in total precipitation depth. Notably, when considering all landslides together (Fig. 3) the precipitation events that triggered landslides at burned sites were significantly smaller than those that triggered landslides at unburned locations (Mann–Whitney test, $95\,\%$ confidence). This difference supports the overarching hypothesis that wildfire does in fact increase landslide susceptibility, since landslides in the period after a fire can be triggered by less precipitation than might normally be required to cause mass movement. An examination of each region separately reveals that the difference in precipitation percentile between burned and unburned sites is present in some regions but not in others (see Fig. 3). The California area (Fig. 3 panel (b)) has a particularly strong signal, whereas tropical regions do not show any significant differences between precipitation at burned and unburned sites or display the reverse effect of higher precipitation percentiles for unburned locations than burned locations.

3.2 Comparison of bootstrapped samples and pre-landslide precipitation

Figure 4 highlights the increase in precipitation in the days before a landslide relative to historical amounts for that location and time of year, i.e., relative to climatology, offering a robust assessment of the landslide precipitation departure. The Mann–Whitney p–values comparing the precipitation record on each day to each of the ~ 100 samples are shown in 4 panels (a)–(g). Examples of the kernel density estimates of each bootstrap sample as compared to the precipitation on the day of the landslide are shown in Fig. 4 panels (h)–(u) to better illustrate the comparisons made by the hypothesis tests in panels (a)–(g). Each orange or purple curve was tested against the black curve to obtain the boxplots of p–values at 0 days before the landslide. A clear difference between burned and unburned sites is shown for the same regions as in Fig. 3, but with the addition of Southeast Asia. Beyond the emergence of a signal in Southeast Asia, additional differences between regions in the timing of

https://doi.org/10.5194/nhess-2021-111
Preprint. Discussion started: 28 April 2021

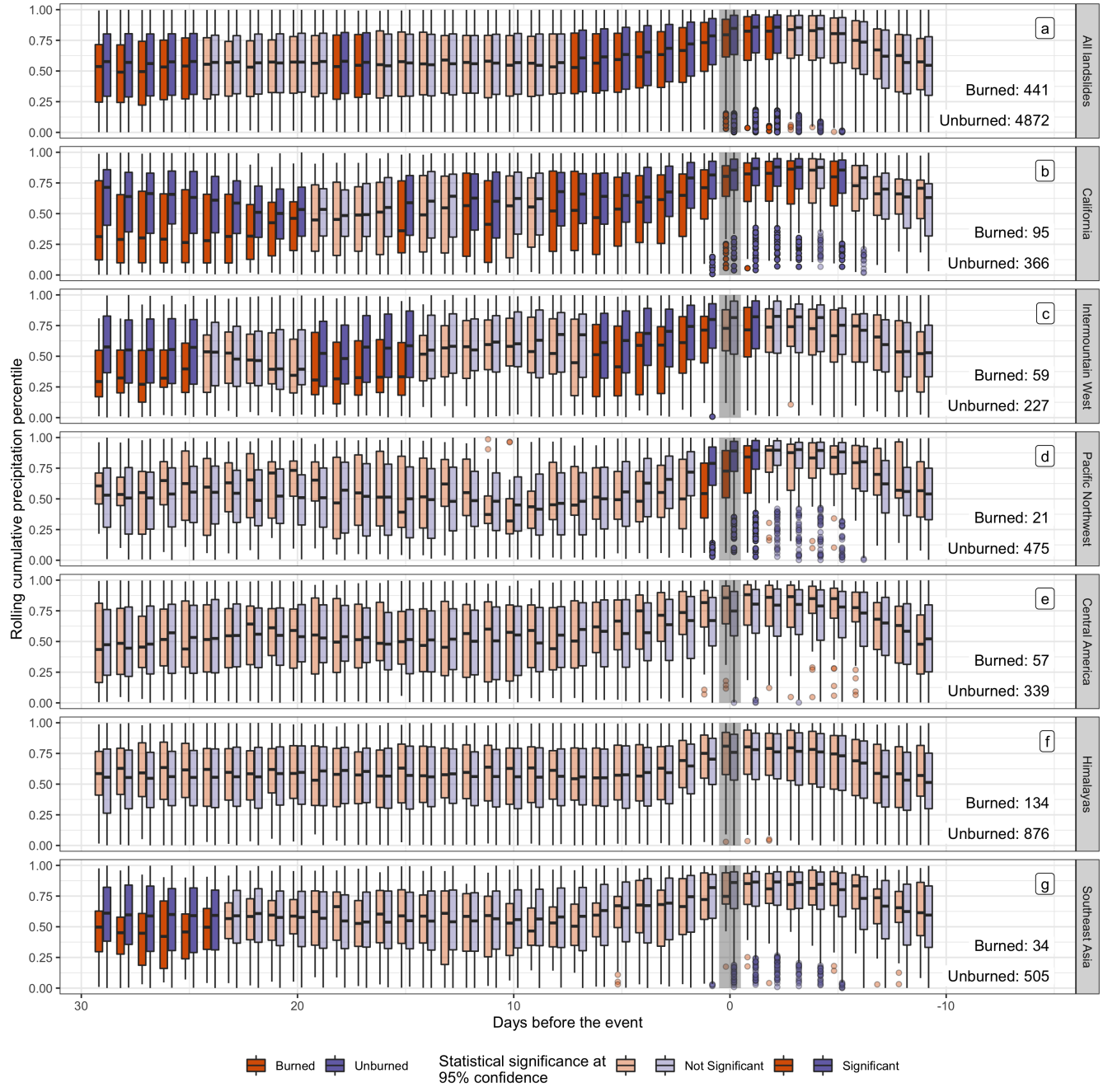

Figure 3. Seven-day precipitation percentile in the lead-up to landslides for all landslides in (a) and for the six individual regions labeled (b)–(g), whether classified as part of one of the regions or not. Days where a significant difference was found between the burned and unburned groups are indicated in bold coloring (Mann–Whitney hypothesis test, $p > 0.05$).

https://doi.org/10.5194/nhess-2021-111
Preprint. Discussion started: 28 April 2021

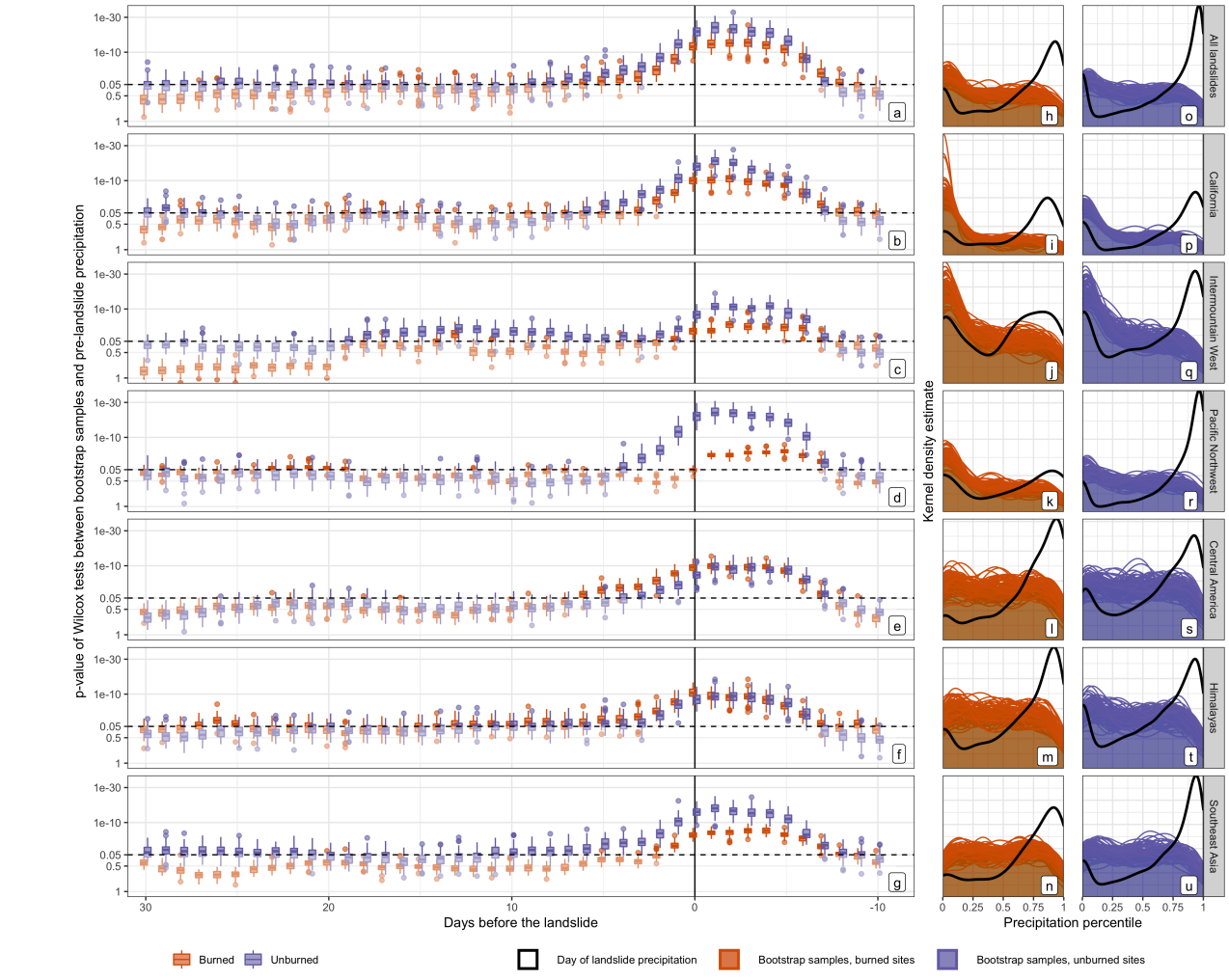

Figure 4. p–values of Mann–Whitney hypothesis tests comparing landslide-triggering precipitation relative to 100 bootstrapped samples ($n \sim 100$ for each sample) drawn from a 38-year precipitation record from the landslide locations. Landslide events have been split into burned and unburned groups (shown in orange and purple respectively) for six regions and for all landslides in the study. Bootstrapped samples were drawn from the same DOY and locations as the landslides but from a randomly selected year. In panels (a)–(g), box plots of p–values represent the degree to which the landslide-triggering precipitation differed from climatological precipitation with lower values indicating a larger difference between the two precipitation distributions. To illustrate whether there are differences between burned and unburned groups when the p–values below 0.05 (significant at $95\,\%$ confidence, shown as a dashed black line), the y–axes are shown with a probit transform to expand that section of the axis. The y–axis has also been inverted so that larger differences in precipitation (lower p–values) are higher on the y–axis for consistency with the percentile plots in Fig. 3. In panels (h)–(u), an example of the kernel density estimate (kde) for day-of-landslide precipitation in black separated by burned and unburned groups is compared with kdes of all bootstrapped samples in orange (burned group) or purple (unburned group).

https://doi.org/10.5194/nhess-2021-111
Preprint. Discussion started: 28 April 2021


Natural Hazards and Earth System Sciences Discussions

precipitation in the period leading up to the landslide are visible in Fig. 4 panels (a)–(g) that were not clear in the precipitation percentile analysis.

Different storm timing is apparent among the regions, with implications for potentially region-specific physical processes associated with landslide triggers. Firstly, in the Himalayas and Southeast Asia (Fig. 4 panels (f) and (g)) precipitation rises at a similar rate for each group, indicating that landslides at burned and unburned locations are triggered by similar precipitation increases. Curiously, the bootstrap analysis reveals a long-term difference between burned sites and unburned sites in the Mann–Whitney p–value for Southeast Asia despite location-specific normalization, suggesting that the landslides at unburned locations might be primarily triggered in years that are wetter than usual on a monthly or possibly seasonal scale. In the Pacific Northwest and California (Fig. 4 panels (d) and (b)), the burned sites exhibit shorter but more intense storms than the unburned sites in the week preceding the landslide. Under the assumption that shorter, more intense storms are associated with runoff-driven landslides while longer storms that allow more time for the soil column to saturate are associated with infiltration-driven landslides, this difference in storm timing suggests that the burned landslide locations are largely runoff-driven while rainfall-triggered landslides at unburned locations are infiltration-driven (Cannon and Gartner, 2005). The Mann–Whitney p–values for the burned group remain well above 0.05 just days before the landslide as the p–value for the unburned group begins to fall. In the Intermountain West (Fig. 4 panel (c)) antecedent precipitation for the burned group is generally characterized by a dry spell going back thirty days or more. Twenty to thirty days before the landslide p–values are consistently above 0.9, suggesting a high likelihood ($> 90\,\%$) that there was less precipitation than usual during that time.

3.3 Landslide and fire seasonality experiment

Figure 5 shows the seasonality of fires and landslides at each site, in addition to the length of time elapsing between the fire and the landslide. Landslides in several regions, especially California and the Himalayas, tend to occur at the same time of year. This time of year, for the regions where it exists, will be referred to as 'landslide season.' Similarly, nearly all of the regions have a fire season, which is most clearly visible in the black rug at the top of each panel in Fig. 5. Figure 5 panel (a) shows that fires occur nearly year-round when considering all regions together, but the other panels in Fig. 5 show that within any particular region, fires occur only during a distinct time of year. However, the delay between fire and landslide is not consistently equal to the length of time between fire season and the following landslide season. The landslides are distributed such that $4854\,\%$ occur within a one year after the fire and at least $10\,\%$ of sites in each region the fire occurred between two and three years before the landslide. Since both landslides and fires have seasonal patterns, the typical delay between fire and landslide for each region appears to be primarily related to the relationship between fire season and landslide season. For example, California has a long fire season and a shorter landslide season, and so when fires occur at the end of winter, immediately after landslide season, there is typically a longer delay before the landslide than when fires occur immediately before landslide season. By contrast, in the Himalayas the delay between fire and landslide is relatively uniform due to a shorter fire season that does not overlap with the landslide season.

Figure 6 shows differences in seasonality between burned and unburned landslide seasonality on the right and the results of the precipitation frequency analysis on the left. While all regions except for Central America (Fig. 6 panel (l)) display some

https://doi.org/10.5194/nhess-2021-111
Preprint. Discussion started: 28 April 2021

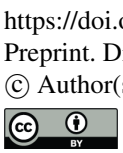

Natural Hazards and Earth System Sciences
Discussions
Open Access
EGU

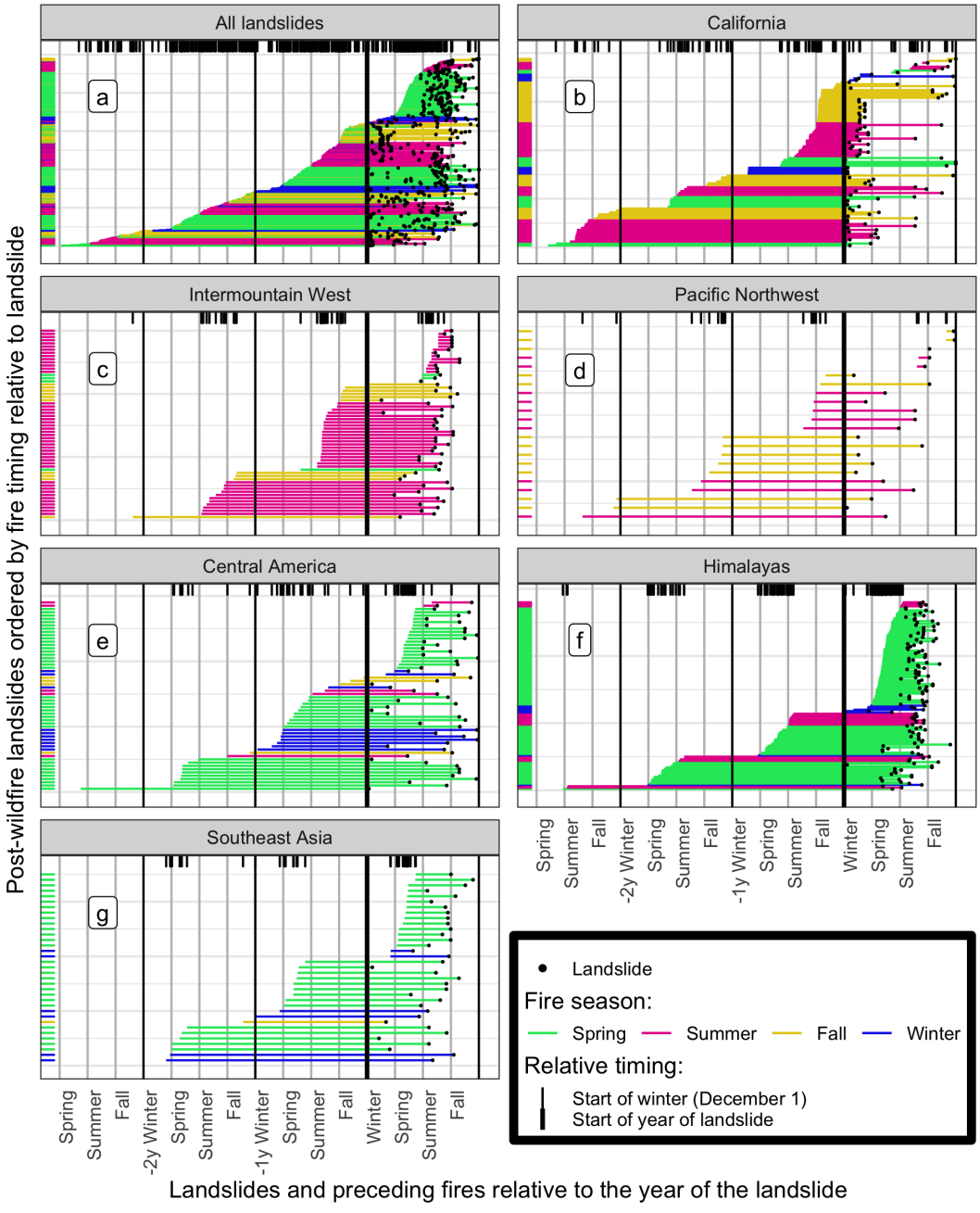

Figure 5. DOY of landslides, DOY of fires, and the length of time in between fire and landslide by region. Black dots on the right show the day of the year the landslide occurred, and horizontal lines represent the duration of time elapsed in between the fire and the landslide. Lines are colored by the season of the fire and are ordered by the day of the fire relative to the landslide. The black lines, or rug, at the top of each panel as well as the colored rug on the left duplicate the day-of-year of the fires to highlight seasonal patterns.

https://doi.org/10.5194/nhess-2021-111
Preprint. Discussion started: 28 April 2021

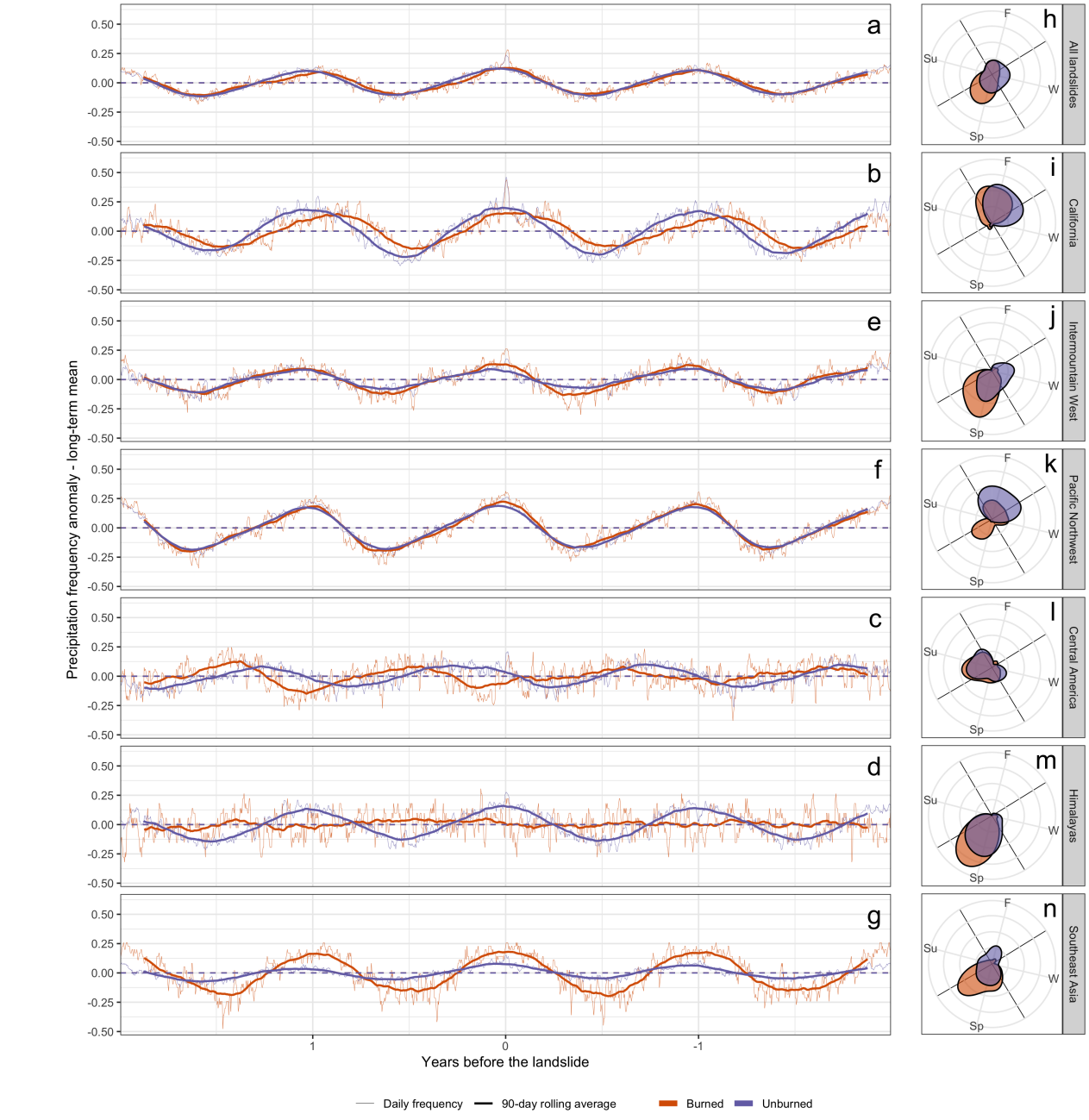

Figure 6. Precipitation frequency anomaly relative to the long-term mean aligned by the landslide date. In panels (a)(g), frequency is shown both daily and smoothed with a 90-day moving average to highlight shifts. The long-term mean has been removed from all the frequency curves. Landslides are in burned and unburned groups for each region separately and for all landslides. In panels (h)–(n), the kernel density estimate of landslides by the time of year is shown for both the burned and unburned groups in a radial plot.

https://doi.org/10.5194/nhess-2021-111
Preprint. Discussion started: 28 April 2021


Natural Hazards and Earth System Sciences
Discussions

kind of shift in seasonality between burned and unburned landslides in right-hand panels of Fig. 6 ((h)–(n)), the magnitudes and directions of these shifts varies by region. Interestingly, the regions with clear shifts in seasonality have shifts of different directions, i.e. earlier or later in the year, and magnitudes, i.e. a few weeks to half a year. In the Southeast Asia (Fig. 6 panel (n)), landslides at burned sites happen in the summer rather than the winter for unburned sites, a 6-month shift. In contrast, landslides in the Intermountain West (Fig. 6 panel (j)), burned landslides appear to happen in the spring while unburned landslides occur in the winter, a 3-month shift later in the year. In California (Fig. 6 panel (i)), by contrast, burned landslides are shifted earlier in the year and by only a few weeks, with both burned and unburned landslides occurring primarily in the fall and early winter. Finally, in the Pacific Northwest (Fig. 6 panel (k)), it appears that some of the burned landslides occur in the usual landslide season of fall and early winter, while another peak lies 6 months away at the beginning of summer.

The precipitation frequency in Fig. 6 panels (a)–(g) highlights differences in when landslides tend to occur relative to the wetter parts of the annual precipitation cycle between burned and unburned groups. A curve for burned sites that is shifted slightly to the right of the corresponding curve for unburned sites, as is the case for the burned group precipitation frequency in the California region (Fig. 6 panel (b)), indicates that burned landslides occurred earlier in the rainy season. In California and the Himalayas (Fig. 6 panels (b) and (f)) burned landslides are clearly shifted to earlier in the time of year with more frequent precipitation, i.e. earlier in the wet season, although the shift is larger in California. This provides evidence confirming our hypothesis that wildfire increases landslide susceptibility in these regions, since it suggests that a smaller precipitation trigger that might be found earlier in a wetter part of the year is required to trigger a landslide after a fire. The Intermountain West (Fig. 6, panel (c)) also has a pronounced seasonal shift, but in this case the shift is much larger, so much so that the burned landslides in this region appear to occur as a result of a large storm in the middle of a dry part of the year. Other regions (Pacific Northwest in panel (d), Southeast Asia in panel (g), and Central America in panel (e)) show differences in the magnitude of the annual cycle in precipitation frequency, but no shift in seasonality. These magnitude changes are not consistent in direction or degree across regions. In Southeast Asia, where Fig. 6 panel (n) shows a shift in seasonality but panel (g) does not show a shift relative to the wetter parts of the year, these results suggest that there could be a spatial or climatic bias to the locations of burned landslides that is causing the seasonal difference.

4 Discussion

The results of this study suggest that while post-wildfire landslides are associated with shifts in the magnitude, timing, and seasonality of storms relative to other landslides, these effects are not consistent across regions. Globally, there are clear differences in the percentiles of landslide-triggering storms (see Fig. 3), with landslides in burned areas often triggered by comparatively smaller storms. This supports the hypothesis that fires increase landslide susceptibility, since a smaller precipitation trigger is sufficient to cause a mass movement. However, this trend is largely driven by the California region and to a lesser extent the Intermountain West and Pacific Northwest of North America. In Central America/Caribbean, Southeast Asia, and the Himalayas the percentiles from both burned and unburned locations increase leading up to the landslide, but there is no significant difference between relative precipitation depths.

https://doi.org/10.5194/nhess-2021-111
Preprint. Discussion started: 28 April 2021


Natural Hazards and Earth System Sciences Discussions

Differences in the landslide-triggering storms relative to their precipitation climatology shown by the bootstrap analysis (Fig. 4) reveal a sharper ramp-up in precipitation for unburned sites leading up to the date of the landslide. This phenomenon again supports the idea that wildfires increase landslide susceptibility. Burned locations in California and the Pacific Northwest appear to be associated with rainfall that began closer to when the landslide occurred (Fig. 4 panels (b) and (d)), suggesting that burned landslides in these regions are potentially caused more often than in unburned locations by runoff from short-duration storms. This result is consistent with previous research suggesting that post-wildfire debris flows are predominantly triggered by runoff-driven erosion as a result of shorter and more intense storms in the Western US (76% Cannon and Gartner, 2005). Contrastingly, burned locations in the Intermountain West (Fig. 4 panel (c)) appear to be particularly susceptible to shorter-duration storms that occur after a dry spell stretching from twenty to thirty days before the landslide and possibly beyond. A similar pattern of low frequency precipitation followed by a sharp spike can be seen in the burned locations in Fig. 6 panel (c). One possible explanation is that dry, recently burned soil is particularly erosive in those areas. These differences are also due in part to the different regional climates, with the California and Pacific Northwest regions having more clearly defined longer-duration rainy seasons, relative to the more variable and sporadic precipitation seasonality of the Intermountain West.

Different combinations of fire season, landslide season, and any overlap between the two may be an important driving factor in the degree to which fires increase landslide susceptibility. For example, in places where the wet season begins towards the end or immediately after fire season, such as the Intermountain West, California, and the Himalayas, the landscape has no time to recover from the fire before landslide season begins and therefore burned locations may be much more susceptible (see Fig. 5 panels (b), (c), and (f)). On the other hand, in regions like the Pacific Northwest, Central America, and Southeast Asia (Fig. 5 panels (d), (e), and (g)), where landslide season is not as well defined, it is more likely that the landscape could at least partially recover before a triggering storm occurs.

Some of the regions that did not display a significant difference in percentile nonetheless showed a shift in the timing of burned landslides relative to their respective annual pattern of precipitation (see Fig. 6 panels (h)–(n)). The various types of shifts in landslide seasonality are likely reflective of the different effect of fires. A shift of the landslide season to slightly earlier in the year, such as was noticeable in California and the Himalayas (see Fig. 6 panels (i) and (m)) supports the hypothesis that wildfire increases landslide susceptibility because it suggests that fewer or smaller precipitation events earlier in the season are sufficient to trigger a landslide. The Intermountain West (Fig. 6 panel (j)) also has a pronounced seasonal shift, but in this case the shift is much larger and in the opposite direction: burned landslides appear to occur an entire season later than unburned landslide, falling in the driest part of the year instead of the wettest. This corresponds to the evidence from the bootstrap analysis suggesting that dried out soil or slow vegetation regrowth may be an important part of the post-wildfire landslide mechanism in this region. Vegetation regrowth as a main control of landslide susceptibility is supported by a study of landslide occurrence in the San Gabriel mountains of the US by Rengers et al. (2020), in which the authors found that hillslopes with slower vegetation regrowth were more likely to have landslides.

A similar trend to the Intermountain West in terms of seasonal shift is visible for some, but not all, of the landslides in the Pacific Northwest (Fig. 6 panel (k)), suggesting perhaps that some of landslides in that region would have been better categorized as part of the Intermountain West region. In Southeast Asia (Fig. 6 panel (n)) there also appears to be a seasonal

https://doi.org/10.5194/nhess-2021-111
Preprint. Discussion started: 28 April 2021


Natural Hazards and Earth System Sciences Discussions

shift similar to that of the Intermountain West, but it is not matched by a shift relative to the annual precipitation frequency pattern (Fig. 6 panel (g)). This suggests that the seasonality "shift" in Southeast Asia is actually a spatial bias as to the climates in which many of the landslides take place. Finally, Central America (Fig. 6 panel (l) has very similar precipitation frequency in burned and unburned locations. Since there is little difference between the precipitation frequency or magnitude (see Figs. 3 panel (e), 6 panel (e)) in this area, it is possible that there are many misidentified 'false positive' post-wildfire landslides in Central America. It is also possible wildfire does not have as much of an effect on landslide susceptibility in that region.

Low landslide location accuracy and lower number of burned landslides may have also contributed to the lack of conclusive results in the Pacific Northwest, Southeast Asia and Central America. The regions outside the US and Canada tended to have less accurate landslide locations, and less accurate locations were also more likely to be marked as burned. This is because larger landslide radii were more likely to contain burned area by chance alone, and hence become 'false positive' post-wildfire landslides, i.e. landslides that occurred nearby but not coincident to a burned area. This idea is supported by the lower cumulative burned fractions within the regions outside the US and Canada (see Fig. 1 panels (c) and (d)). However, the degree to which fires and landslides are statistically linked also contributes to the rate of false positives. Some regions may have many false positive burned landslides because there was a larger percentage of low accuracy locations, or alternatively because there was no significant increase in the probability that a landslide would occur in a burned location. Such a low posterior landslide probability given that a fire has occurred would tend to greatly increase the number of false positive burned areas by decreasing the probability that a landslide occurred in the burned section of the landslide radius, thus negating the effects of larger landslide buffers. In order to estimate which effect between location accuracy and changes in post-wildfire landslide susceptibility was the most important in each region, a validation of precisely which landslides were truly post-wildfire would be needed. However, this type of validation falls outside the scope of this analysis. Future studies using visible and other satellite imagery to pinpoint landslide locations and dates could help clarify the post-wildfire posterior landslide probability by essentially eliminating the location error. Furthermore, there is a body of research that uses GIS data such as slope or underlying lithography in combination with a statistical model like a classification tree or logistic regression to assess landslide hazards (e.g. Felicísimo et al., 2013; Lee, 2007; Ohlmacher and Davis, 2003), including some focused on post-wildfire landslides (Cannon et al., 2010). The introduction of such control datasets of confirmed unburned landslide locations would also allow the use of additional variables like slope, land use, and aridity index to be incorporated into a model as part of an assessment of which properties of sites have the greatest influence on changes in landslide susceptibility at burned sites.

5 Conclusions

Clear differences were shown between rainfall-triggered landslides at unburned and unburned locations in the magnitude of precipitation triggers, the seasonality of landslides, and the timing of triggering storms. These findings suggest that wildfires increase susceptibility to landslides, especially in regions of the Western US. However, they also suggest that post-wildfire landslides are not a spatially uniform phenomenon. Both the mechanisms by which burned landslides are triggered and the degree to which wildfire increases susceptibility varies by region.

https://doi.org/10.5194/nhess-2021-111
Preprint. Discussion started: 28 April 2021

The precipitation percentile immediately before a landslide was found to be smaller at burned locations for all regions combined, as well as for the California, Intermountain West, and Pacific Northwest regions, but not for the others. This result suggests greater landslide susceptibility in those three regions following a wildfire. In California and the Pacific Northwest, landslide-triggering storms tended to be shorter at burned locations, suggesting that these landslides are more often runoff-driven than landslides at unburned locations. In contrast, in the Intermountain West burned landslide locations appear to be characterized by a dry spell followed by a sharp uptick in precipitation, suggesting that burned and dry soil may be the most vulnerable to extreme erosion in that region. Finally, shifts in landslide seasonality were noted in every region except Central America, although the characteristics of these shifts were not consistent among regions. In some regions such as California and the Himalayas, landslides at burned locations occurred earlier in the wet season, suggesting greater susceptibility to landslides caused by fire. In other regions such as the Intermountain West and Southeast Asia, landslide seasonality was shifted by 3 or 6 months, suggesting that the physical mechanisms causing landslides at burned and unburned locations in these regions are entirely different. For example, we posit that post-wildfire landslides in these regions may be caused by isolated intense thunderstorms on dry soil while landslides at unburned locations are caused by saturation of the soil.

Developing a better understanding of the ways in which landslide hazards vary around the world is important for mitigation efforts as well as predicting how landslide hazards will respond to a changing climate. Data acquisition is a major barrier to this type of global analysis of landslide statistics. Both precipitation and burn status are major sources of uncertainty in this analysis due to imprecise landslide locations. This work offers new insights into the role of wildfire on landslide susceptibility, representing a first step towards broader understanding of regional triggering mechanisms. Future efforts should incorporate additional high-accuracy landslide locations (e.g. ~ 500m) that are more representatively distributed around the globe to further advance understanding into landslide responses across climates and regions.

Author contributions. Elsa Culler and Ben Livneh designed the experiments in consultation with all co-authors. Balaji Rajagopalan assisted with the design of the statistical analysis and Kristy Tiampo aided in the analysis of the landslide triggers. Elsa Culler processed the data, developed the model code and performed the statistical analysis. Elsa Culler prepared the manuscript with contributions from all co-authors.

Competing interests. The authors declare that they have no conflict of interest.

Acknowledgements. This research was funded by NASA IDS grant 16-IDS16-0075, The Interaction of Mass Movements with Natural Hazards Under Changing Hydrologic Conditions.

https://doi.org/10.5194/nhess-2021-111
Preprint. Discussion started: 28 April 2021

References

Budimir, M. E. A., Atkinson, P. M., and Lewis, H. G.: A Systematic Review of Landslide Probability Mapping Using Logistic Regression, Landslides, 12, 419–436, https://doi.org/10.1007/s10346-014-0550-5, 2015.

Burrows, K., Walters, R. J., Milledge, D., Spaans, K., and Densmore, A. L.: A New Method for Large-Scale Landslide Classification from Satellite Radar, Remote Sensing, 11, 237, https://doi.org/10.3390/rs11030237, 2019.

Cannon, S. H. and DeGraff, J.: The Increasing Wildfire and Post-Fire Debris-Flow Threat in Western USA, and Implications for Consequences of Climate Change, in: Landslides – Disaster Risk Reduction, pp. 177–190, Springer, Berlin, Heidelberg, https://doi.org/10.1007/978-3-540-69970-5_9, 2009.

Cannon, S. H. and Gartner, J. E.: Wildfire-Related Debris Flow from a Hazards Perspective, in: Debris-Flow Hazards and Related Phenomena, edited by Jakob, M. and Hungr, O., Springer Praxis Books, pp. 363–385, Springer, Berlin, Heidelberg, https://doi.org/10.1007/3-540-27129-5_15, 2005.

Cannon, S. H., Gartner, J. E., Wilson, R. C., Bowers, J. C., and Laber, J. L.: Storm Rainfall Conditions for Floods and Debris Flows from Recently Burned Areas in Southwestern Colorado and Southern California, Geomorphology, 96, 250–269, https://doi.org/10.1016/j.geomorph.2007.03.019, 2008.

Cannon, S. H., Gartner, J. E., Rupert, M. G., Michael, J. A., Rea, A. H., and Parrett, C.: Predicting the Probability and Volume of Postwildfire Debris Flows in the Intermountain Western United States, GSA Bulletin, 122, 127–144, https://doi.org/10.1130/B26459.1, 2010.

Deckmyn, A., Becker, R. A., Wilks, A. R., Brownrigg, R., and Minka, T. P.: Maps: Draw Geographical Maps, 2018.

DeGraff, J. V., Cannon, S. H., and Gartner, J. E.: The Timing of Susceptibility to Post-Fire Debris Flows in the Western United States, Environmental and Engineering Geoscience, 21, 277–292, https://doi.org/10.2113/gseegeosci.21.4.277, 2015.

Donnellan, A., Parker, J., Milliner, C., Farr, T. G., Glasscoe, M., Lou, Y., Zheng, Y., and Hawkins, B.: UAVSAR and Optical Analysis of the Thomas Fire Scar and Montecito Debris Flows: Case Study of Methods for Disaster Response Using Remote Sensing Products, Earth and Space Science, 5, 339–347, https://doi.org/10.1029/2018EA000398, 2018.

Ebel, B. A., Moody, J. A., and Martin, D. A.: Hydrologic Conditions Controlling Runoff Generation Immediately after Wildfire, Water Resources Research, 48, https://doi.org/10.1029/2011WR011470, 2012.

Felicísimo, Á. M., Cuartero, A., Remondo, J., and Quirós, E.: Mapping Landslide Susceptibility with Logistic Regression, Multiple Adaptive Regression Splines, Classification and Regression Trees, and Maximum Entropy Methods: A Comparative Study, Landslides, 10, 175–189, https://doi.org/10.1007/s10346-012-0320-1, 2013.

Froude, M. J. and Petley, D. N.: Global Fatal Landslide Occurrence from 2004 to 2016, Natural Hazards and Earth System Sciences, 18, 2161–2181, https://doi.org/10.5194/nhess-18-2161-2018, 2018.

Funk, C., Peterson, P., Landsfeld, M., Pedreros, D., Verdin, J., Shukla, S., Husak, G., Rowland, J., Harrison, L., Hoell, A., and Michaelsen, J.: The Climate Hazards Infrared Precipitation with Stations—a New Environmental Record for Monitoring Extremes, Scientific Data, 2, 1–21, https://doi.org/10.1038/sdata.2015.66, 2015.

Gartner, J. E.: Relations between Wildfire Related Debris-Flow Volumes and Basin Morphology, Burn Severity, Material Properties and Triggering Storm Rainfall, M.A., University of Colorado at Boulder, United States – Colorado, 2005.

Gartner, J. E., Cannon, S. H., Helsel, D. R., and Bandurraga, M.: Mutivariate Statistical Models for Predicting Sediment Yields from Southern California Watersheds, Open-File Report, U.S. Geological Survey, Reston, VA, 2009.

https://doi.org/10.5194/nhess-2021-111
Preprint. Discussion started: 28 April 2021

Gartner, J. E., Cannon, S. H., and Santi, P. M.: Empirical Models for Predicting Volumes of Sediment Deposited by Debris Flows and Sediment-Laden Floods in the Transverse Ranges of Southern California, Engineering Geology, 176, 45–56, https://doi.org/10.1016/j.enggeo.2014.04.008, 2014.

Giglio, L., Boschetti, L., Roy, D. P., Humber, M. L., and Justice, C. O.: The Collection 6 MODIS Burned Area Mapping Algorithm and Product, Remote Sensing of Environment, 217, 72–85, https://doi.org/10.1016/j.rse.2018.08.005, 2018.

Harp, E. L., Keefer, D. K., Sato, H. P., and Yagi, H.: Landslide Inventories: The Essential Part of Seismic Landslide Hazard Analyses, Engineering Geology, 122, 9–21, https://doi.org/10.1016/j.enggeo.2010.06.013, 2011.

Highland, L. and Bobrowsky, P.: The Landslide Handbook: A Guide to Understanding Landslides, Circular 1325, United States Geological Survey, Reston, VA, 2008.

James, A. L. and Roulet, N. T.: Antecedent Moisture Conditions and Catchment Morphology as Controls on Spatial Patterns of Runoff Generation in Small Forest Catchments, Journal of Hydrology, 377, 351–366, https://doi.org/10.1016/j.jhydrol.2009.08.039, 2009.

Kirschbaum, D. and Stanley, T.: Satellite-Based Assessment of Rainfall-Triggered Landslide Hazard for Situational Awareness, Earth's Future, 6, 505–523, https://doi.org/10.1002/2017EF000715, 2018.

Kirschbaum, D., Kapnick, S. B., Stanley, T., and Pascale, S.: Changes in Extreme Precipitation and Landslides Over High Mountain Asia, Geophysical Research Letters, 47, e2019GL085 347, https://doi.org/10.1029/2019GL085347, 2020.

Kirschbaum, D. B., Adler, R., Hong, Y., Hill, S., and Lerner-Lam, A.: A Global Landslide Catalog for Hazard Applications: Method, Results, and Limitations, Natural Hazards, 52, 561–575, https://doi.org/10.1007/s11069-009-9401-4, 2010.

Kirschbaum, D. B., Adler, R., Hong, Y., Kumar, S., Peters-Lidard, C., and Lerner-Lam, A.: Advances in Landslide Nowcasting: Evaluation of a Global and Regional Modeling Approach, Environmental Earth Sciences, 66, 1683–1696, https://doi.org/10.1007/s12665-011-0990-3, 2012.

Klose, M.: Introduction, in: Landslide Databases as Tools for Integrated Assessment of Landslide Risk, edited by Klose, M., Springer Theses, pp. 1–24, Springer International Publishing, Cham, https://doi.org/10.1007/978-3-319-20403-1_1, 2015a.

Klose, M.: Landslide Databased - State of Research and the Case of Germany, in: Landslide Databases as Tools for Integrated Assessment of Landslide Risk, edited by Klose, M., Springer Theses, pp. 25–43, Springer International Publishing, Cham, https://doi.org/10.1007/978-3-319-20403-1_2, 2015b.

Lee, S.: Application and Verification of Fuzzy Algebraic Operators to Landslide Susceptibility Mapping, Environmental Geology, 52, 615–623, https://doi.org/10.1007/s00254-006-0491-y, 2007.

Lee, S. and Pradhan, B.: Landslide Hazard Mapping at Selangor, Malaysia Using Frequency Ratio and Logistic Regression Models, Landslides, 4, 33–41, https://doi.org/10.1007/s10346-006-0047-y, 2007.

Liu, Y., Goodrick, S., and Heilman, W.: Wildland Fire Emissions, Carbon, and Climate: Wildfire–Climate Interactions, Forest Ecology and Management, 317, 80–96, https://doi.org/10.1016/j.foreco.2013.02.020, 2014.

Lu, P., Casagli, N., Catani, F., and Tofani, V.: Persistent Scatterers Interferometry Hotspot and Cluster Analysis (PSI-HCA) for Detection of Extremely Slow-Moving Landslides, International Journal of Remote Sensing, 33, 466–489, https://doi.org/10.1080/01431161.2010.536185, 2012.

Martha, T. R., van Westen, C. J., Kerle, N., Jetten, V., and Vinod Kumar, K.: Landslide Hazard and Risk Assessment Using Semi-Automatically Created Landslide Inventories, Geomorphology, 184, 139–150, https://doi.org/10.1016/j.geomorph.2012.12.001, 2013.

Meena, S. R. and Tavakkoli Piralilou, S.: Comparison of Earthquake-Triggered Landslide Inventories: A Case Study of the 2015 Gorkha Earthquake, Nepal, Geosciences, 9, 437, https://doi.org/10.3390/geosciences9100437, 2019.

https://doi.org/10.5194/nhess-2021-111
Preprint. Discussion started: 28 April 2021

Mezaal, M. R., Pradhan, B., Sameen, M. I., Mohd Shafri, H. Z., and Yusoff, Z. M.: Optimized Neural Architecture for Automatic Landslide Detection from High-Resolution Airborne Laser Scanning Data, Applied Sciences, 7, 730, https://doi.org/10.3390/app7070730, 2017.

Moody, J. A., Martin, D. A., Haire, S. L., and Kinner, D. A.: Linking Runoff Response to Burn Severity after a Wildfire, Hydrological Processes, 22, 2063–2074, https://doi.org/10.1002/hyp.6806, 2018.

Neary, D. G., Ryan, K. C., and DeBano, L. F.: Wildland Fire in Ecosystems: Effects of Fire on Soils and Water, Tech. Rep. RMRS-GTR-42-V4, U.S. Department of Agriculture, Forest Service, Rocky Mountain Research Station, Ft. Collins, CO, https://doi.org/10.2737/RMRS-GTR-42-V4, 2005.

Nefeslioglu, H. A., Sezer, E., Gokceoglu, C., Bozkir, A. S., and Duman, T. Y.: Assessment of Landslide Susceptibility by Decision Trees in the Metropolitan Area of Istanbul, Turkey, Mathematical Problems in Engineering, https://doi.org/10.1155/2010/901095, 2010.

Nyman, P., Sheridan, G. J., Smith, H. G., and Lane, P. N. J.: Evidence of Debris Flow Occurrence after Wildfire in Upland Catchments of South-East Australia, Geomorphology, 125, 383–401, https://doi.org/10.1016/j.geomorph.2010.10.016, 2011.

Ohlmacher, G. C. and Davis, J. C.: Using Multiple Logistic Regression and GIS Technology to Predict Landslide Hazard in Northeast Kansas, USA, Engineering Geology, 69, 331–343, https://doi.org/10.1016/S0013-7952(03)00069-3, 2003.

Reneau, S. L., Katzman, D., Kuyumjian, G. A., Lavine, A., and Malmon, D. V.: Sediment Delivery after a Wildfire, Geology, 35, 151–154, https://doi.org/10.1130/G23288A.1, 2007.

Rengers, F. K., McGuire, L. A., Oakley, N. S., Kean, J. W., Staley, D. M., and Tang, H.: Landslides after Wildfire: Initiation, Magnitude, and Mobility, Landslides, 17, 2631–2641, https://doi.org/10.1007/s10346-020-01506-3, 2020.

Rupert, M. G., Cannon, S. H., and Gartner, J. E.: Using Logistic Regression To Predict the Probability of Debris Flows Occurring in Areas Recently Burned By Wildland Fires, Open-File Report, U. S. Geological Survey, 2003.

Schuster, R. and Highland, L.: Socioeconomic and Environmental Impacts of Landslides in the Western Hemisphere, Open-File Report, U. S. Geological Survey, 2001.

Shakesby, R. A. and Doerr, S. H.: Wildfire as a Hydrological and Geomorphological Agent, Earth-Science Reviews, 74, 269–307, https://doi.org/10.1016/j.earscirev.2005.10.006, 2006.

Shakesby, R. A., Coelho, C. D. A., Ferreira, A. D., Terry, J. P., and Walsh, R. P. D.: Wildfire Impacts on Soil-Erosion and Hydrology in Wet Mediterranean Forest, Portugal, International Journal of Wildland Fire, 3, 95–110, https://doi.org/10.1071/wf9930095, 1993.

Spiker, E. C. and Gori, P. L.: National Landslide Hazards Mitigation Strategy - A Framework for Loss Reduction, Circular 1244, U. S. Geological Survey, 2002.

Spittler, T.: Fire and Debris Flow Potential of Winter Storms, in: Brushfires in California Wildlands: Ecology and Resource Management, pp. 113–120, International Association of Wildland Fire, Fairfield, Washington, 1995.

Staley, D., Negri, J., Kean, J., Tillery, A., and Youberg, A.: Updated Logistic Regression Equations for the Calculation of Post-Fire Debris-Flow Likelihood in the Western United States, Open-File Report, U. S. Geological Survey, 2016.

van Westen, C. J., van Asch, T. W. J., and Soeters, R.: Landslide Hazard and Risk Zonation—Why Is It Still so Difficult?, Bulletin of Engineering Geology and the Environment, 65, 167–184, https://doi.org/10.1007/s10064-005-0023-0, 2006.